Microstructure-based analysis of cone penetration tests in snow

Isabel Peinke[1,*], Pascal Hagenmuller[1], Edward Andò[2], Frédéric Flin[1], Guillaume Chambon[3], Jacques Roulle[1]

[1]*Météo-France - CNRS, CNRM/CEN, Grenoble, France*
[2]*UGA, CNRS, Grenoble INP, 3SR, F-38000 Grenoble, France*
[3]*UGA, Irstea, UR ETGR, 38402 Saint Martin d'Hères, France*

ABSTRACT: Cone penetration tests (CPT) are common to measure vertical profiles of the snow hardness. The SnowMicroPenetrometer (SMP) is a high-resolution CPT, which allows to link the measured penetration strength, especially its high-frequency fluctuations, to microstructural snow characteristics. With a non-homogeneous Poisson point process (NHPP) we are able to get estimations of the number of bonds, breaking due to the cone indentation and estimations of the strength of the bonds. We did combined measurements of SMP and tomography. Therefore, several samples, spanning different snow types were imaged twice, once before and once after a CPT. With a new algorithm, we are able to recover and quantify the displacements between the pre-CPT and post-CPT images. The resulting 3D displacement field will give us information about the bonds which break and what happens around the SMP tip. With the calculation of the radial displacement, we are able to estimate the size of the compaction zone and the number of the displaced grains. We can compare this number to the number of broken bonds, estimated by the NHPP model.

Keywords: Snow microstructure, X-Ray tomography, grain tracking, SnowMicroPenetrometer

1. INTRODUCTION

Snow avalanche forecast requires a good knowledge of vertical layering of the snowpack (e.g. Schweizer et al., 2003). Penetration tests are simple measurements to get an information of the vertical snow hardness profile. The ramsond was in the 1930s the first cone penetration test (CPT) used in snow. Nowadays, a high-resolution penetrometer is the SnowMicroPenetrometer (Schneebeli and Johnson, 1998). It measures the penetration resistance every 4 μm and is supposed to give thus information on the snow microstructure and the micromechanical properties (e.g. Johnson and Schneebeli, 1999). Several studies were conducted to estimate micromechanical parameters like the rupture event intensity, microscopic rupture force and deflection at rupture (e.g. Löwe and Herwijnen, 2012).

It is known that, in front of penetrometers a compaction zone is formed, which cannot be neglected for the interpretation of the signal (e.g. Herwijnen, 2013). Herwijnen (2013) did PIV experiments to get the displacement field around the tip and also computed microtomography (μCT) to get the compaction zone. For the experiments they modified the SMP and were not able to do measurements at the same time. We propose combined measurements of SMP and μCT to have high-resolution images of the area around the tip to better understand the interaction between the tip and the grains. This is needed to better understand and interpret the recorded signal in terms of micromechanical properties. Therefore μCT images were taken before and after the SMP measurement and the grains were tracked with a combination of digital image correlation (DIC) and an individual grain tracking method.

2. MATERIAL AND METHODS

2.1. Sample preparation and experimental set-up

The snow samples, covering 3 different snow types (Tab. 1), were sieved directly in the sample holders for the micro computed tomography (μCT) at an ambient temperature of -10°C. During the following experiments, the temperature were hold constant. These sample holders were cylinders, measuring 2 cm in diameter and height. To ensure that the snow grains and the bonds between the grains did not evolve significantly during the experiment, a minimal rest time of 24 hours between sieving and experiments was chosen. Each snow sample was imaged twice, once before and once after the penetration test. The penetration tests were performed with the SnowMicroPenetrometer (SMP version 4, Schneebeli and Johnson (1998)). We modified the SMP tip, such that only the tip penetrated into the snow (Fig 1). This modification was necessary, as the sample size was with 2 cm almost the same size of the rod (1.8 cm). After the measurement the SMP tip was not directly removed, but about 1 hour afterwards. This rest time was chosen to enable the

*Corresponding author address: Isabel Peinke, Météo-France/CEN, 1441 rue de la piscine, F-38400 St Martin d'Hères, France; email: isabel.peinke@meteo.fr

Table 1: Physical properties of the snow samples used in this study. The used grain types were according to Fierz et al. (2009): large rounded grains (RGlr), rounded grains (RG), and depth hoar (DH).

Snow type	Density (kg m^{-3})	SSA (m^2 kg^{-1})
RGlr	496 ± 2	14.0 ± 0.4
RG	315 ± 2	24.2 ± 0.5
DH	361 ± 2	17.0 ± 0.5

grains to sinter and thus to avoid that they fall into the hole, when the tip is removed. The imaging was done in a tomographic cabin (Rx-Solutions) using CellDyM (Calonne et al., 2015) to maintain the cold. The images have a voxel size of 15 μm.

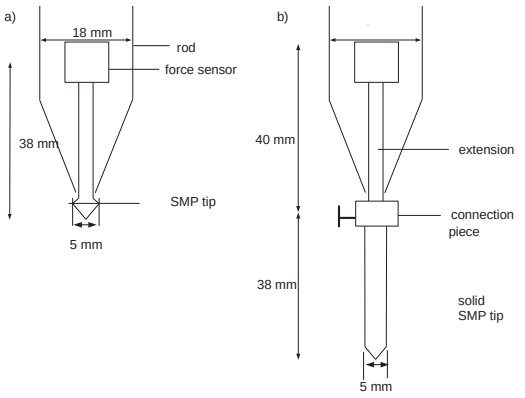

Figure 1: Experimental set-up: a) scheme of the original SMP tip, b) scheme of the for the experiments modified tip.

2.2. Image analysis and grain tracking

All images were segmented into grains with the method from Hagenmuller et al. (2014). Then, we developed a method to get the displacements of the grains. For small displacements, we used digital image correlation (DIC), which used the initial and final μCT images and the grain segmentation of the initial image to find the displacement and rotation of the grains between the images. A correlation coefficient (CC) gives information on the quality of these estimations. For our images, we defined a grain as found, if the CC was larger than 0.75. With this method we were able to detect the grains, which moved less than 10 voxels. The advantage of this method is, that only the grain segmentation of the first image is needed and thus it is independent of errors due to different segmentations of the two images. The grains of both images, which were not found with the DIC method, were isolated in order to apply a morphological based tracking on them. For further tests, we started by taking different thresholds to choose possible grain couples, i.e. one grain in each of the two segmented images, which might be the same grain. As morphological criterion, we chose a maximal volume difference and elongation difference of 50%. Further, a displacement criteria on the horizontal displacement (i.e. the displacement in x- and y-direction) was applied: small horizontal displacement (< 100 voxel) can be in all directions, whereas larger displacements were only possible to be in outward-direction. On the resulting grain couples, we computed the eigenvectors and aligned them in all possible ways. Then, their overlap was calculated, that had to be above 70% to be accepted. On the potential couples, which were found after all these criteria, we applied a DIC to verify if the grain couple was effectively the same snow grain. If the CC of these potential couples was higher than 0.75 ,the grains in the two images were considered as being the same snow grain. The grains that were not found at that point, were moved and turned like their closest neighbours. Then, a DIC was applied to check if the grains did really move like this. Here again, the CC threshold was set to 0.75.

2.3. SMP analysis

The macroscopic penetration force $F(z)$, measured with the SMP, was analysed with a non-homogeneous shot noise model (NHPP, Peinke et al. submitted). This model considers the macroscopic force $F(z)$ to be a superposition of spatially uncorrelated and randomly distributed rupture events (e.g. Johnson and Schneebeli, 1999; Marshall and Johnson, 2009). One event is assumed to correspond to a single bond rupture. The events can occur at different depths, but they are assumed to be identical and to have an elastic-brittle behaviour. The two microstructural properties describing these ruptures are the deflection length δ and the rupture force f. The intensity λ_z, which can vary with depth, consists of the number of events per penetration increment and is described by a Poisson distribution. To apply the NHPP, the relative variations of $\lambda_z(z)$ over an interval of length δ should be negligible. Assuming this for our snow, the micromechanical properties are given by:

$$f = \frac{3}{2}\overline{\widetilde{F}^2}, \qquad \delta = -\frac{3}{2}\frac{C(0)}{C'(0)}, \qquad \lambda_z(z) = \frac{4}{3\delta}\frac{\kappa_1(F)}{\overline{\widetilde{F}^2}} \tag{1}$$

where $\bar{\bullet}$ stand for the mean over depth, $\widetilde{F}$ is the stationarized force given by $\widetilde{F} = (F - \kappa_1(F))/\kappa_1(F)^{1/2}$. $\kappa_1(F)$ is approximated by $\overline{F}$ on a running window of width Δz=3 mm. Note that this approximation requires the variation of the intensity λ_z to be approximately linear over intervals of width Δz.

Table 2: Estimated micromechanical properties of the snow samples used in this study. The micromechanical rupture force (f), the deflection at rupture (δ) and the mean rupture event intensity ($\overline{\lambda}$).

Snow type	f (N)	δ (mm)	$\overline{\lambda}$ (mm^{-1})
RGlr	0.177	0.094	43
RG	0.014	0.025	2 125
DH	0.038	0.069	188

3. RESULTS

3.1. Micromechanical Properties with NHPP

Figure 2 shows the measured force profiles of 3 different samples (Fig. 2a) and their corresponding estimated rupture event intensities (Fig. 2b). The mean microscopic rupture force f, mean deflection at rupture δ and the mean intensity $\overline{\lambda}$ are given in tab. 2. The large rounded grains (RGlr) exhibit the highest penetration forces, whereas the rounded grains (RG) and depth hoar (DH) exhibit similar smoothed values of the penetration force. The micromechanical properties show nevertheless clear differences between these two snow types. The intensity (λ) displays the lowest values for the RGlr followed by the DH and RG. Whereas, the microscopic rupture force (f) and the deflection at rupture (δ, see Tab.2) exhibit the smallest values for RG, then DH and the highest one for RGlr.

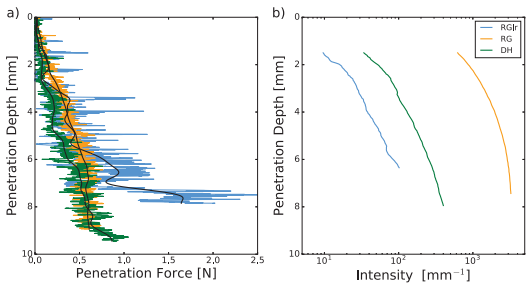

Figure 2: SMP force profiles (a) and their estimated rupture event intensities (b) for three different snow types (RGlr, RG, DH). The SMP profiles show the penetration force (coloured line) superposed with their smoothed profile (black line), with a Gaussian filter with a standard deviation of 0.2 mm.

3.2. Displacement field

Table 3 gives information about the total number of grains and how many we were able to track. The main part of the grains was found with the DIC, and 3-6% of the total number with the tracking. But these percentage is important as it contains the grains with the large displacements.

The computed displacement fields and the radial displacements are presented in Fig. 3. The figures on the left side (Fig. 3 a,c,e) displays a x-slice of the initial grains (contours) with their total displacement (coloured areas) for the three different snow types (RGlr, RG and DH). The arrows represent the y and z component of the displacement vectors for the grains in this slice. The graphs on the right side (Fig. 3 b,d,f) display the radial displacement versus their initial distance to the center (radial position) for all tracked grains. The values are smoothed with a Gaussian filter of a standard deviation of 20 points. Table 4 display the estimation of the compaction zone (CZ) radius from the radial displacement curves. From this, we calculated the volume fraction of the CZ with respect to the volume of the sample. Therefore, we assumed a cylindrical CZ, and we took the height of the penetration measurement. Combining the volume fraction and the total number of grains in the sample from the segmentation, we can calculate grain intensity of the displaced grains, i.e. the mean number of grains contained in a one millimetre high CZ.

Table 3: Overview of the number of grains, that were found by the different tracking methods.

Snow	total grains	grains found with DIC	grains found with tracking
RGlr	17 318	16 037 (93%)	732 (4%)
RG	73 648	63 940 (84%)	4 018 (5%)
DH	28 803	24 143 (87%)	1 637 (6%)

Table 4: Information of compaction zone, estimated from the images. It shows its radius, the approximate volume fraction of the CZ in respect to the sample volume and an estimation of the number of displaced grains per millimetre of CZ height.

Snow	Radius (mm)	Volume fraction (%)	Grains (mm^{-1})
RGlr	4.6	11.9	262
RG	5.3	16.0	1 320
DH	6.1	22.2	677

All the displacement fields show downwards movements in the lower part and upwards movements in the upper part. This upwards movement is the most developed for the RGlr. The CZ radii are between 4.6 and 6.1 mm (i.e. 1.8 to 2.4 times the tip radius): the RGlr exhibits the smallest CZ, whereas the DH the largest one. The mean rupture intensity, estimated by the NHPP model, displays the smallest values for RGlr and the largest ones for RG. This corresponds to the same order, that we can find if we calculate the number of grains in the CZ from the μCT images.

4. DISCUSSION AND CONCLUSIONS

The NHPP model enables the estimation of micromechanical properties of the snow samples. For example, it was possible to distinguish the proper-

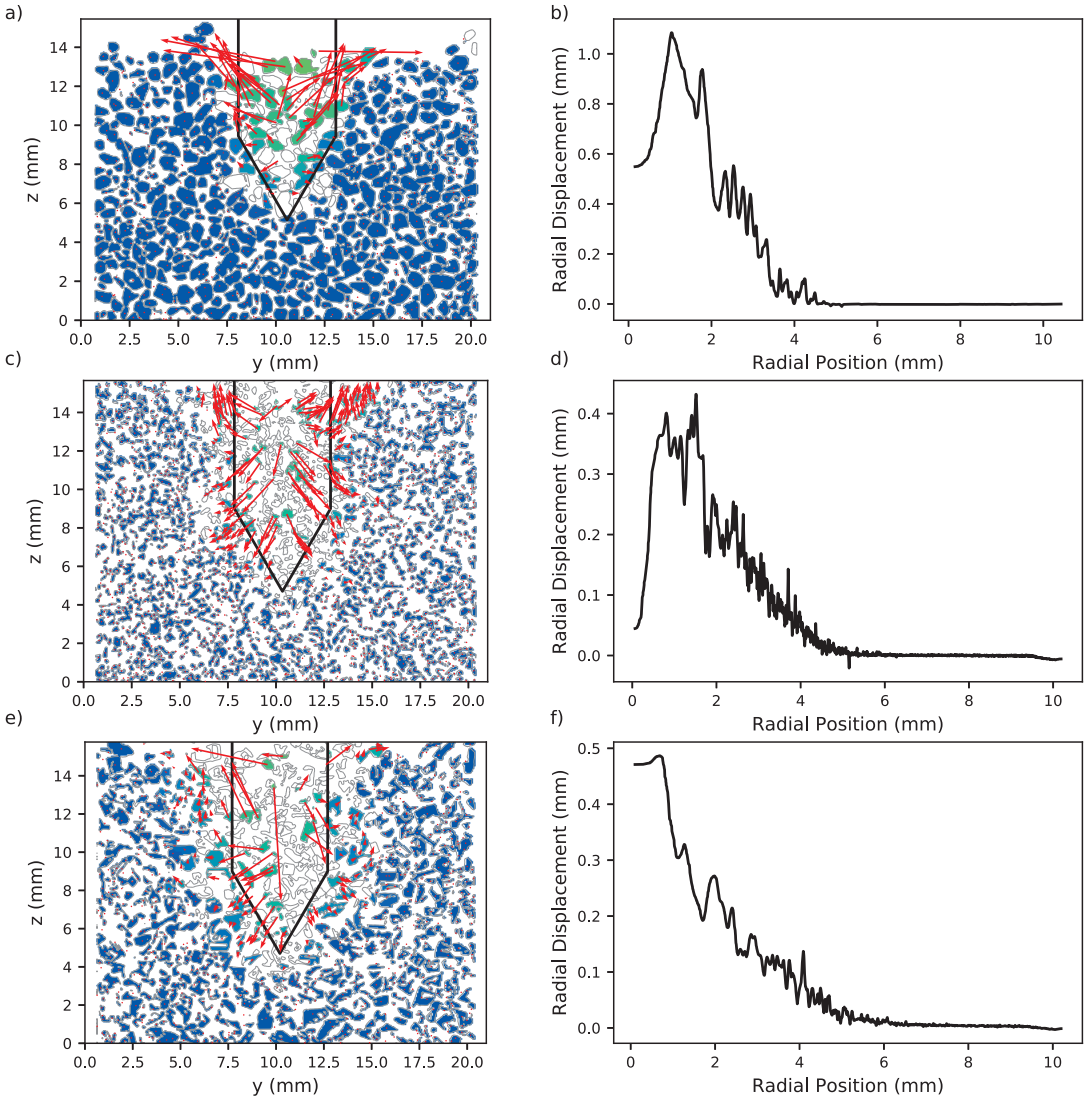

Figure 3: Displacement field and radial displacement of the initial grains for the three snow types RGlr (a,b), RG (c,d), and DH (e,f). On the left side (a,c,e): In gray the contours of the grains, the colors show the absolute displacement, and the arrows show the displacement components of y and z. On the right side (b,d,f): the radial displacement versus the radial position (i.e. distance to the center).

ties of DH and RG, which showed similar mean penetration forces. The NHPP model estimated less and stronger bonds for DH than for RG (i.e. a lower rupture event intensity and a higher microscopic rupture force). For the RGlr the fewest bond ruptures with the highest rupture forces were detected.

The combination of discrete image correlation (DIC) and a morphological grain tracking enables to follow grains even with large displacements. About 90% of the grains of three different snow types could be tracked, among them about 50% of the grains with large displacements, were detected with the grain tracking. The advantage of the DIC is, that the result is independent of the final segmentation of the grains. Nevertheless, it is only possible to detect small displacements with the DIC. A morphological grain tracking is thus needed to get larger displacements. This method is dependent on the quality of the grain segmentation itself, which is one possible reason why we detected about 50% of the large displacements. A better grain segmentation should lead to a better result. With the reconstructed dis-

placement fields of the RGlr, DH, and RG we thus present, to our knowledge the first study, that is based on a grain tracking method to reconstruct the displacements of single grains due to a cone indentation in snow. Indeed, earlier studies either showed the compaction zone with μCT or analysed the displacement field with 2D PIV (e.g. Floyer and Jamieson, 2006; Herwijnen, 2013).

The reconstructed displacement fields for all three grain types (RGlr, DH, RG) show an upwards movement, at least for the upper regions. Especially for the RGlr, almost all grains moved upwards. This displacement could be due to its high density, which would mean that almost no compaction is possible and the grains are pushed upwards. This would also explain that we observed more downward movements for the other grain types. Another reason could be due to the removing of the SMP tip. If the grains stick to the tip, they would be lifted with it.

The radial displacement fields (Fig. 3 b,d,f) enabled us to estimate an approximate radius of the compaction zone (CZ). The radius of the compaction zone was found to be about two times the tip radius, which is in agreement with the literature (e.g. Herwijnen, 2013). The smallest CZ concerned the RGlr, followed by the RG and DH. Further, we were able to calculate the number of grains displaced per millimetre of CZ height. This displacement intensity is the smallest for the RGlr, followed by the DH and RG. The same order can be found comparing the rupture event intensity, estimated by the NHPP model. Nevertheless, a quantitative comparison of these two methods gives no clear result. For example the NHPP model predicts more rupture events than displaced grains for the RG while it is the inverse case for RGlr and DH. This direct link has to be interpreted carefully, as the quantities are not the same, e.g. one displaced grain does not automatically correspond to one broken bond. Besides, errors in segmentation, like an oversegmentation are not taken into account. Additionally, the NHPP gives just an estimation of the micromechanical properties, and no quantitative study exists to evaluate them. To better interpret and compare these results, it would be interesting to have the complete compaction zone and the number and size of the broken bonds calculated from the segmented μCT images and link them directly to the micromechanical properties estimated by the NHPP.

These combined SMP and μCT experiments give a new insight to the displacement field of snow after a cone indentation. It can be linked to existing statistical micromechanical models to interpret the SMP signal, like the non-homogeneous Poisson point model. Nevertheless, it would be interesting to have the complete displacement field with the number and size of the broken bonds.

ACKNOWLEDGEMENT

We thank S. Morin, L. Arnaud and C. Geindreau for fruitful discussions. CNRM/CEN is part of LabEX OSUG@2020 (ANR10 LABX56). Irstea and 3SR are part of LabEX TEC21 (ANR11 LABX30). This work was partly supported by the European Space Agency under ESTEC Contract No. 4000112698/14/NL/LvH.

REFERENCES

Calonne, N., Flin, F., Lesaffre, B., Dufour, A., Roulle, J., Puglièse, P., Philip, A., Lahoucine, F., Geindreau, C., Panel, J.-M., Rolland du Roscoat, S., and Charrier, P. (2015). CellDyM: A room temperature operating cryogenic cell for the dynamic monitoring of snow metamorphism by time-lapse X-ray microtomography. *Geophys. Res. Lett.*, 42(10):3911–3918.

Fierz, C., Armstrong, R. L., Durand, Y., Etchevers, P., Greene, E., McClung, D. M., Nishimura, K., Satyawali, P. K., and Sokratov, S. A. (2009). The international classification for seasonal snow on the ground. *Tech. Doc. Hydrol., 83, UNESCO, Paris*.

Floyer, J. A. and Jamieson, J. B. (2006). Empirical analysis of snow deformation below penetrometer tips. In *Proceedings of the International Snow Workshop*, pages 555–561, Telluride, Colorado.

Hagenmuller, P., Chambon, G., Flin, F., Morin, S., and Naaim, M. (2014). Snow as a granular material: assessment of a new grain segmentation algorithm. *Granular Matter*, 16(4):421–432.

Herwijnen, A. V. (2013). Experimental analysis of snow micropenetrometer (SMP) cone penetration in homogeneous snow layers. *Can. Geotech. J.*, 50:1044–1054.

Johnson, J. and Schneebeli, M. (1999). Characterizing the microstructural and micromechanical properties of snow. *Cold Reg. Sci. Technol.*, 30:91–100.

Löwe, H. and Herwijnen, A. (2012). A Poisson shot noise model for micro-penetration of snow. *Cold Reg. Sci. Technol.*, 70:62–70.

Marshall, H.-P. and Johnson, J. (2009). Accurate inversion of high-resolution snow penetrometer signals for microstructural and micromechanical properties. *J. Geophys. Res.*, 114:F04016.

Schneebeli, M. and Johnson, J. (1998). A constant-speed penetrometer for high-resolution snow stratigraphy. *Ann. Glaciol*, 26:107–111.

Schweizer, J., Jamieson, J. B., and Schneebeli, M. (2003). Snow avalanche formation. *Rev. Geophys.*, 41(4):1016.